Supporting Information

CO residence time modulates multi-carbon formation rates in a zero-gap Cu based CO_2 electrolyzer

Siddhartha Subramanian[*], *Jesse Kok, Pratik Gholkar, Asvin Sajeev Kumar, Hugo-Pieter Iglesias van Montfort, Ruud Kortlever, Atsushi Urakawa, Bernard Dam and Thomas Burdyny*[*]

Corresponding author email: s.s.subramanian@tudelft.nl and T.E.Burdyny@tudelft.nl

Materials for Energy Conversion and Storage (MECS), Department of Chemical Engineering, Faculty of Applied Sciences, Delft University of Technology, van der Maasweg 9, 2629 HZ Delft, The Netherlands.

Gas diffusion electrode architecture

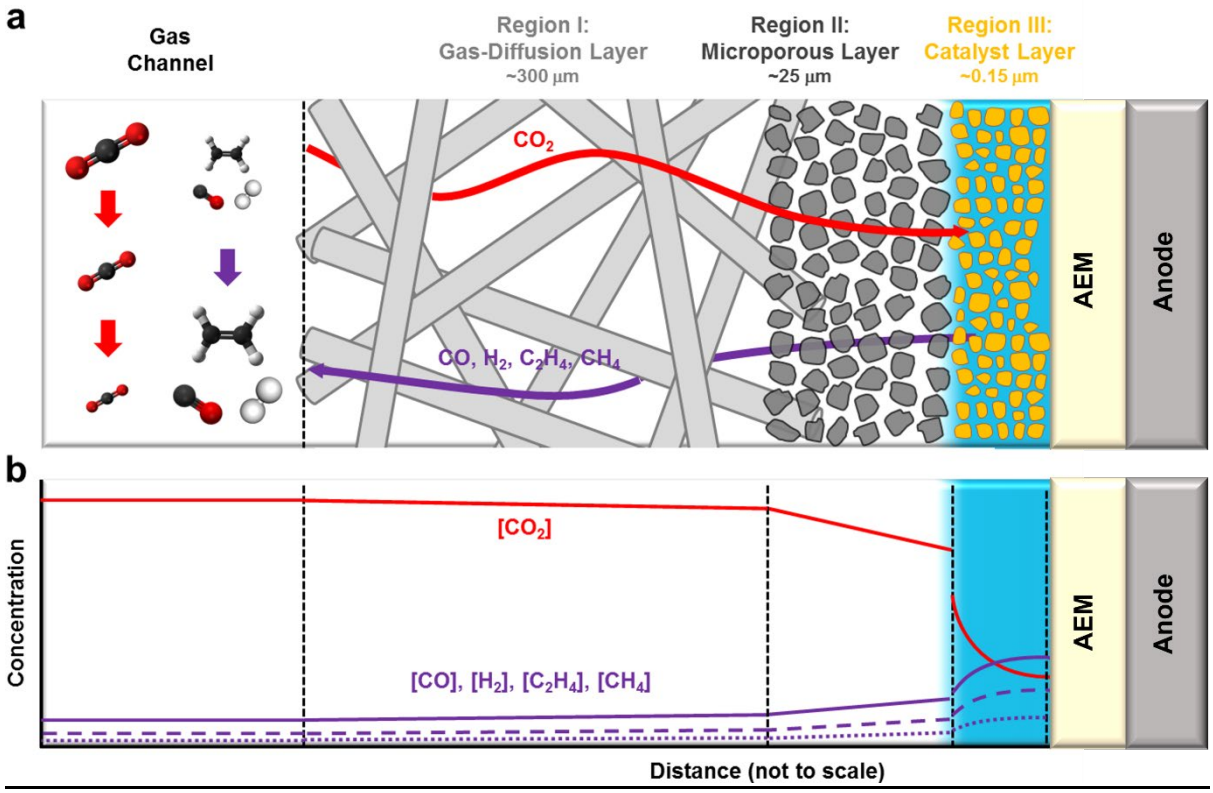

Supplementary Figure 1: Schematic of a gas diffusion electrode (GDE) architecture in an anion exchange MEA configuration. Shown here are the concentration gradients of various species inside the GDE.

Residence time distribution (RTD) measurements using mass spectrometry.

RTD measurements were performed using a Omnistar Pfeiffer Vacuum mass spectrometer with a time resolution of 100 ms. The schematic of the tracer injection system is shown in Supplementary Figure 2. A pneumatic valve was used to switch the two gas streams, one containing the tracer (5 % CO in He) and the other containing pure He gas. The 5% CO in He (95%) gas was used as tracer since its common practice to use a carrier gas for avoiding signal saturation of the mass spectrometer.

As shown in Supplementary Figure 2, the check valve depending on the position, switches the gas streams either to the cathode side of the MEA cell or to the exhaust. A LabVIEW program was used to control the injection and turn off for a fixed duration. For the pulse tracer tests, the tracer was injected for 30 s. For the negative tracer tests, the tracer was injected until the reactor reached saturation and turned off thereafter to record the release of the tracer.

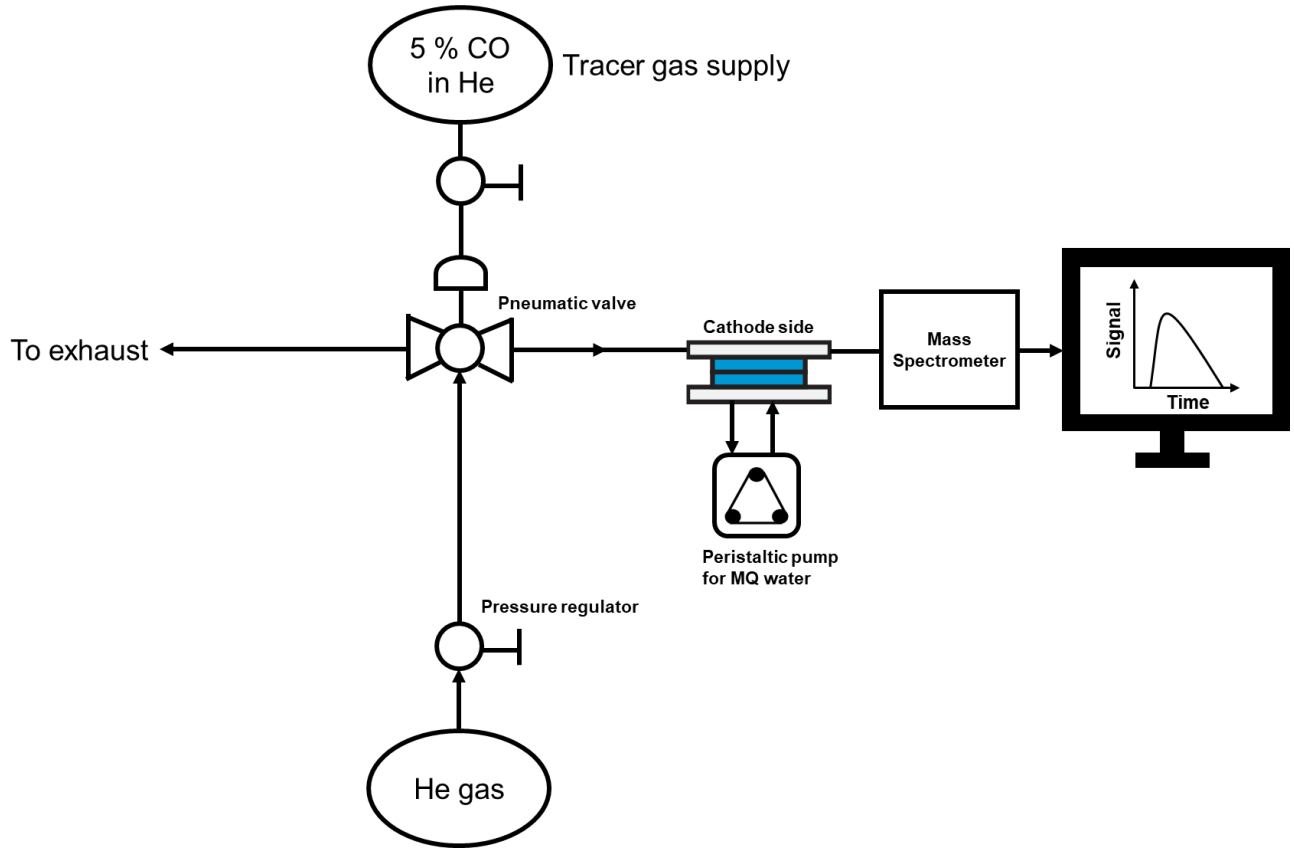

Supplementary Figure 2. Simplified process flow diagram of the RTD system used in the study.

Residence time distribution (RTD) measurements

All RTD tests were performed using commercially purchased carbon based GDL (Sigracet 39 BC) with a microporous layer. Two tests were performed to elucidate the differences between the dry and wetted MPL cases. In the first case, MEA cells were assembled similar to a CO_2 electrolyzer with carbon GDL, Sustainion AEM, Ni foam anode and the two gaskets for both sides. MQ water was constantly flowed at the anode compartment to keep the membrane wetted during RTD tests. At the cathode side, CO tracer was injected to monitor the RTD measurements.

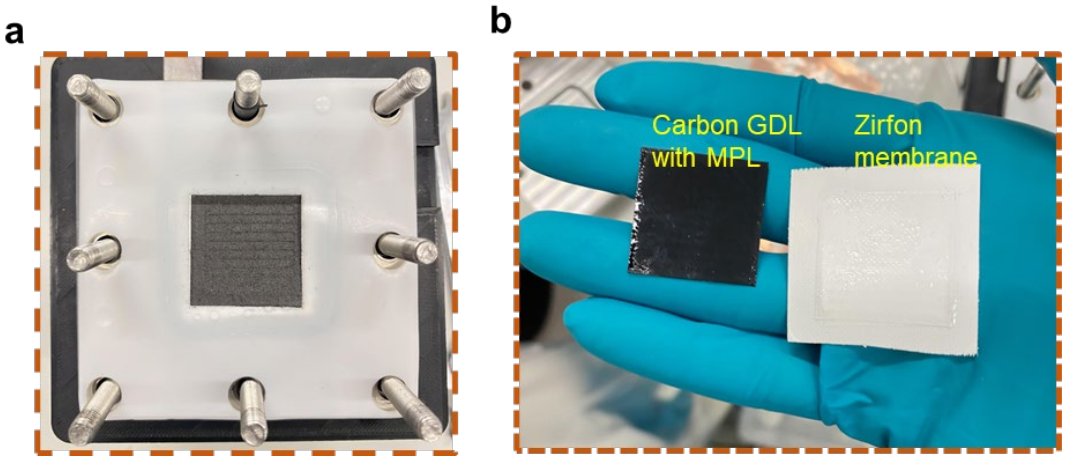

Supplementary Figure 3. (a) Images of Sigracet 39 BC carbon GDL and the MEA setup used in the RTD measurements. (b) Snapshots of MPL side of the carbon GDL and Zirfon membrane post RTD experiments.

In the second type of test, a pretreated Zirfon membrane was pressed on top of the microporous layer side of the GDL inside the MEA cell (Supplementary Figure 3b). Since water was flowing at the other compartment (anode side on Ni foam), porous Zirfon membrane was wetted and acted as a reservoir of water in contact with the carbon GDL at the cathode. This then mimicked a 'wetted catalyst layer' during real ECO_2 R experiments. In both these tests, Ni foam and two gaskets (Silicone for Ni and PTFE for GDL) were used to maintain actual compression occurring in the CO_2 electrochemical tests. For all tests, a non-reactive tracer (5% CO in He gas) was used. Pulse and negative tracer tests were performed for varied inlet flowrates and two flow field patterns (serpentine and parallel).

For these non-electrochemical RTD measurements using Zirfon, we used water as the anolyte to prevent any crystallization of salt at the anode and prevent any electrolyte solution (KOH) from entering the mass spectrometer in vapor phase. Additionally, we do not expect to see a difference when using water or KOH as anolyte as the surface tension of water is relatively constant.

Calculation of mean residence time

Mean residence time of the tracer inside the reactor was calculated for the pulse RTD tests for the 10 and 50 sccm flowrates. For the pulse RTD measurements, the RTD curves with the normalized tracer vs time were first plotted. To eliminate the contribution from the tubing to the reactor, we performed RTD measurements without the MEA cell to measure the 'blank' test. Time taken for the tracer signal to exit during the blank test was then subtracted from the original MEA cell pulse RTD tests. From the resulting plot, the mean residence time was calculated using Eq. S1.

$$t_{mean} = \frac{\sum t_i C_i}{\sum C_i} \quad \text{(S1)}$$

Here t represents the time, C- normalized tracer concentration, *i* represents the 'i^{th}' the data point in the concentration vs time plot.

Differences between gas and liquid phase pulse RTD measurements

Pulse RTD measurements performed with the non-wetted sigracet GDL (without Zirfon membranes) showed faster times for the tracer to exit the reactor. Supplementary Figure 4 shows the pulse RTD measurements for serpentine flow channel performed at 10 sccm with and without the Zirfon membrane in contact with the MPL side of GDL.

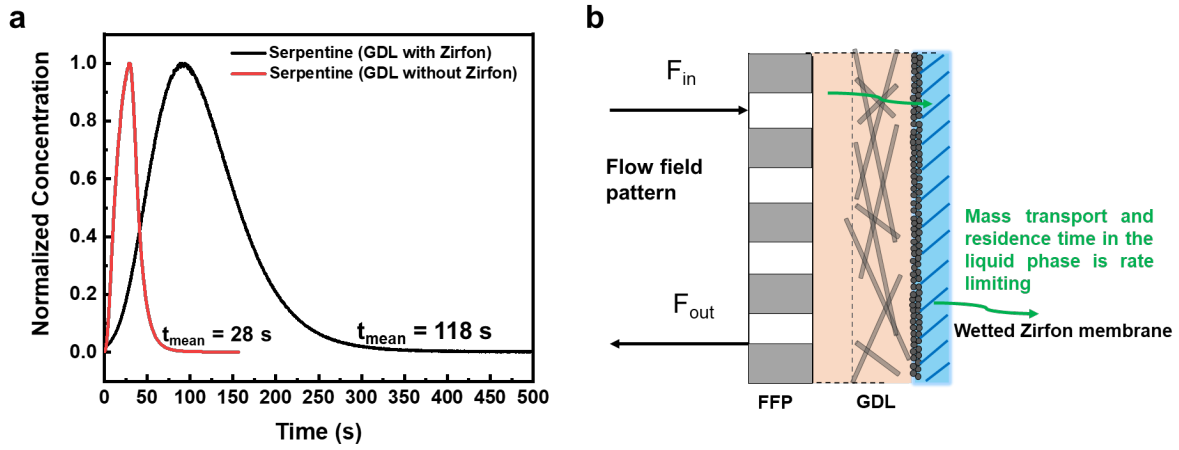

Supplementary Figure 4. (a) RTD pulse tracer output for an inlet flowrate of 10 sccm using serpentine flow field pattern. Black curve shows results for tests with Zirfon membrane placed on top of carbon GDL. Red curve shows output for carbon GDL without Zirfon membrane. (b) Schematic of the wetted zirfon membrane in contact with the GDL creating a reservoir of liquid where mass transport is rate limiting.

The mean residence time of the tracer in the first case without Zirfon membrane is only 28 s. Whereas, for the carbon GDL placed in contact with the Zirfon membrane, the calculated mean residence time comes out to be 118 s. This enhanced residence time with the Zirfon membrane clearly shows that the residence time differences for the flowrates and flow fields stems from the mass transport differences in the liquid phase. Hence, mass transport from the liquid phase of the catalyst is rate limiting during ECO_2R which is why the differences in product distribution are observed for the various flowrates and gas flow field patterns.

In addition to this difference in mean residence time, another evidence supporting this rate limiting step is the shape of the RTD curves as shown in Supplementary Figure 4. The red curve (without

Zirfon) is more sharper than the black curve case (with Zirfon membrane). This clearly shows the delayed residence time occurs in the liquid region in direct contact with the MPL side of the GDL.

Differences between gas and liquid phase negative tracer measurements

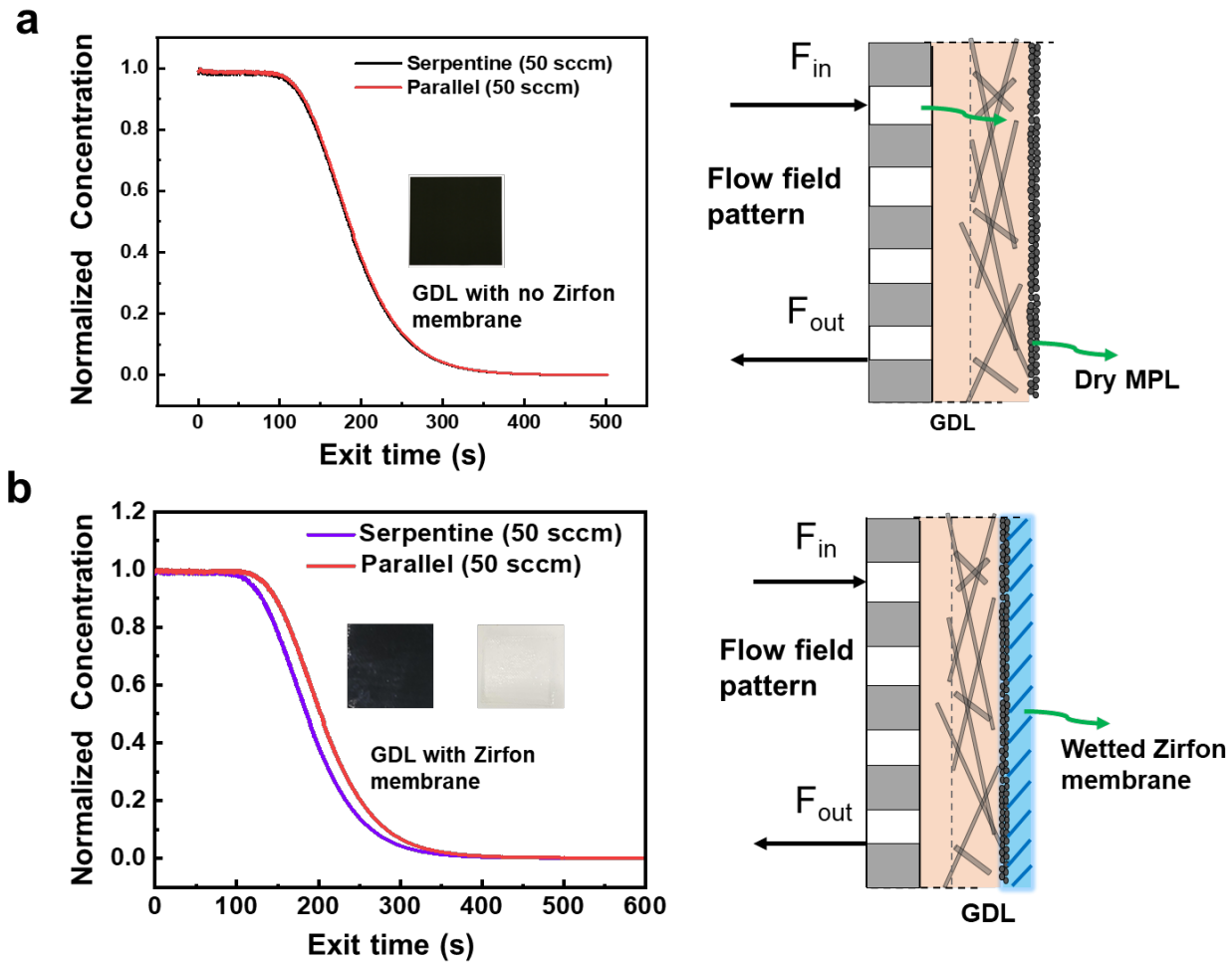

Supplementary Figure 5. Negative tracer results for the serpentine and parallel FFP at an inlet flowrate of 50 sccm without (a) Zirfon membrane pressed against the carbon GDL, (b) with Zirfon membrane pressed against the carbon GDL.

Comparison of negative tracer measurements with Zirfon membrane for both FFP

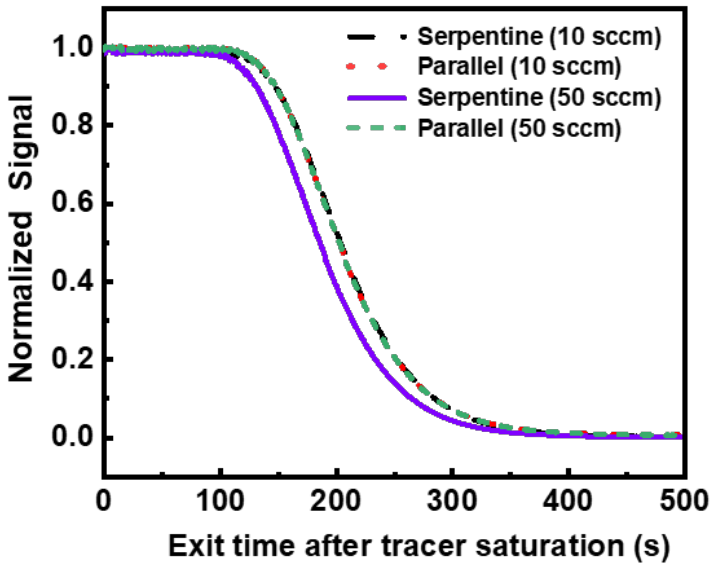

Supplementary Figure 6. Negative tracer results for the serpentine and parallel FFP at an inlet flowrate of 10 and 50 sccm with a wetted Zirfon membrane pressed against the carbon GDL.

Comparison of pulse tracer measurements with Zirfon membrane for parallel FFP

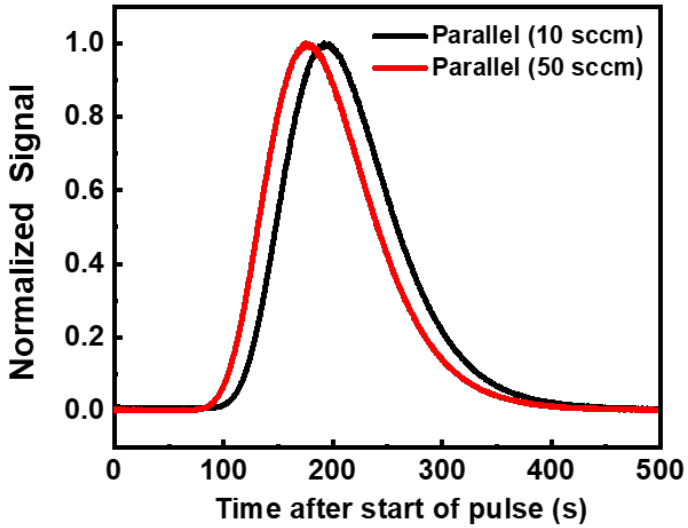

Supplementary Figure 7. Pulse RTD results of the parallel flow field pattern at an inlet flowrate of 10 and 50 sccm with a wetted Zirfon membrane pressed against the carbon GDL.

Negative tracer measurements with Cu coated carbon GDL at 200 mA/cm^2

Since the Zirfon membrane used here has a 500 micron thickness which is thicker than the actual thickness of electrolyte film thickness on top of Cu catalyst layer in real ECO_2R conditions, we repeated negative tracer RTD tests using real Cu GDE under an applied current density of 200 mA/cm^2, using 99.99% Ar as the tracer gas. A pneumatic valve was used to switch the two gas streams, one containing the tracer(99.99% Ar) and the other containing pure He gas both fed at a flowrate of 50 SCCM. Ni foam was used as the anode and 0.5 M KOH was used as anolyte throughout the measurements. Sustainion AEM was used to separate the Ni foam and Cu GDE similar to ECO_2RR and ECOR tests.

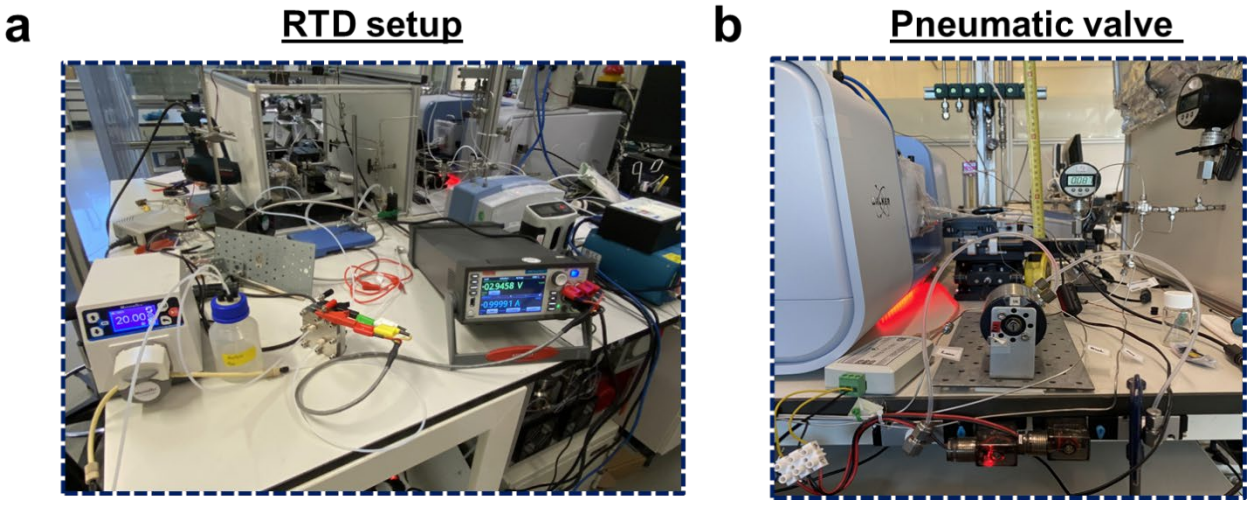

Supplementary Figure 8. (a) Setup used for RTD tests for a Cu GDE under an applied geometric current density of 200 mA/cm^2 and Ar as the tracer gas. (b) The pneumatic valve used to switch between He and Ar (tracer) during the measurements.

RTD of H_2 gas from water electrolysis with a Cu GDE for serpentine flow field design

Additionally, we performed an electrochemical RTD experiment at 200 mA/cm^2 utilizing a configuration and catalyst equal to the CO2RR tests (GDL, sputtered Cu layer, Sustainion AEM, Ni foam anode and 0.5 KOH anolyte). The only difference was using argon as a feed gas instead of CO_2, thus producing H_2 within the catalyst layer. We chose H_2 instead of CO_2 due to the overlapping signals of CO and C_2H_4 due to the similar molecular weights. We then measured the signal of H_2, and the time it took from generation to measurement in the mass spectrometer. Comparing the 10 and 50 SCCM serpentine flow field cases, we then observed a 14 s delay was observed for H_2 between 10 and 50 SCCM cases indicating the increased residence time of products caused by the lower flow rates. These experiments support the use of a Zirfon membrane to mimic the catalyst layer of a GDE under an applied potential.(See Supplementary Figure 9).

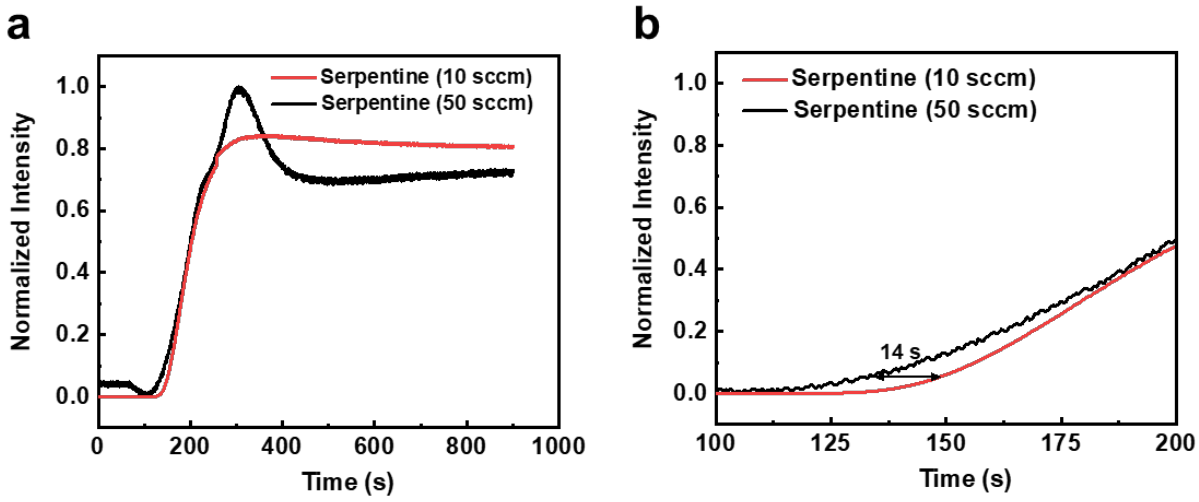

Supplementary Figure 9. Comparison of RTD curves of H_2 gas generated on a sputtered Cu catalyst layer on top of Sigracet 38 BC carbon GDL using serpentine flow field at the cathode and under an applied geometric current density of 200 mA/cm^2 similar to actual CO_2RR

conditions reported in this work. 0.5 M KOH was used as the anolyte with a Ni foam electrode as the anode and Sustainion AEM to separate the two electrodes.

Experimental setup for CO_2 electrolysis

All experiments were performed in a custom-made membrane electrode assembly (MEA) cell comprising of a pin type flow field on the anode and different flow field patterns at the cathode. Electrolysis tests were performed for 1hr and pristine Cu GDE were used for each test. Sigracet 38 BC gas diffusion layers (GDL) of 5.06 cm^2 area (2.25 cm x 2.25 cm) was used as the porous transport layer. Cu catalysts were deposited on top of microporous layer of GDL by direct current magnetron sputtering under 3 μbar Ar flow at 20 sccm to form a uniform film of 100 nm. Nickel foam (3 cm x 3 cm, Recemat BV) was used as the anode. Cu coated GDL and Ni foam were combined with an oversized 16 cm^2 (4cm x 4cm) Sustainion anion exchange membrane (X37-50 Grade RT) to assemble the MEA. 0.5 M KOH solution was fed at the anode at a constant flow rate of 20 ml/min and recirculated using a peristaltic pump (Supplementary Figure 10).

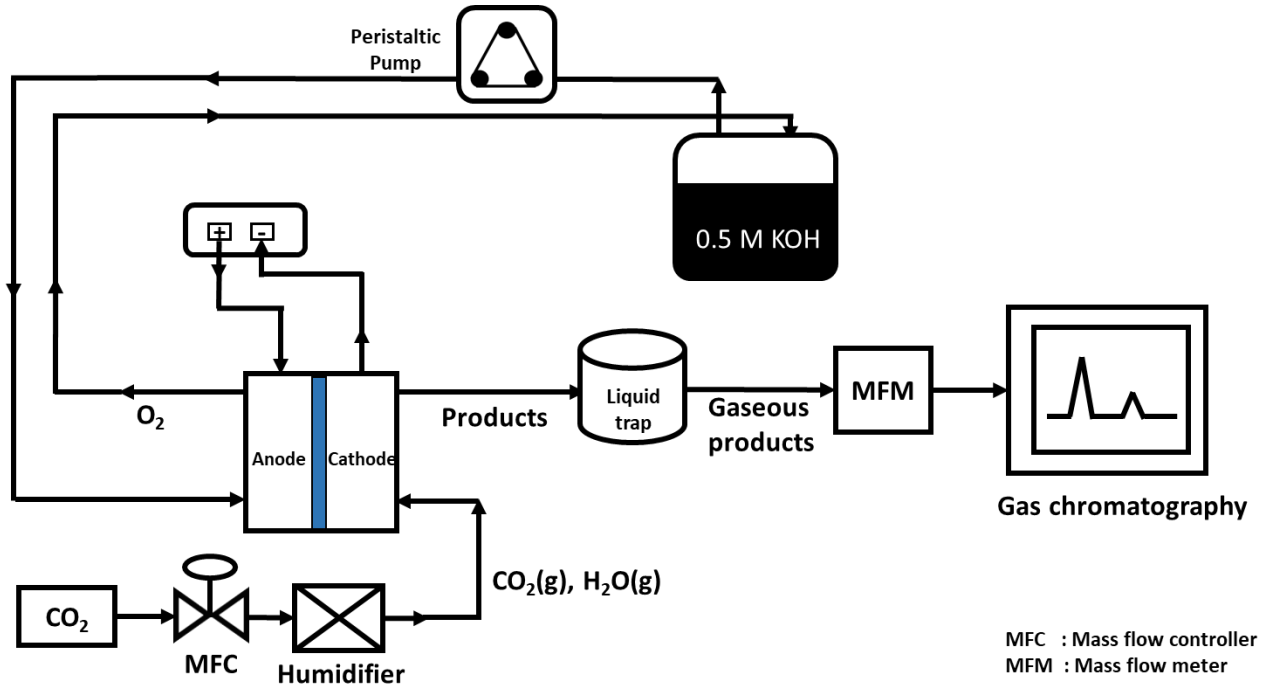

Supplementary Figure 10: Flow diagram of the experimental setup used for CO_2 electroreduction in an exchange MEA.

Different CO_2 flowrates were used and the humidity at the inlet was measured to be 75%. Electrolysis at a geometric current density of 200 mA/cm^2 was performed under various operating conditions. Gas

product quantification was performed by measuring outlet gas flowrates using a mass flow meter (MFM) followed by a gas chromatography (GC) with periodic injections every 5 minutes.

Electrochemical reactions at the cathode

$$CO_2 + H_2O + 2e^- \rightarrow CO + 2OH^- \quad \text{(S2)}$$

$$CO_2 + 6H_2O + 8e^- \rightarrow CH_4 + 8OH^- \quad \text{(S3)}$$

$$2CO_2 + 8H_2O + 12e^- \rightarrow C_2H_4 + 12OH^- \quad \text{(S4)}$$

$$2CO_2 + 9H_2O + 12e^- \rightarrow C_2H_5OH + 12OH^- \quad \text{(S5)}$$

$$2CO_2 + 6H_2O + 8e^- \rightarrow CH_3COO^- + 7OH^- \quad \text{(S6)}$$

$$3CO_2 + 13H_2O + 18e^- \rightarrow C_3H_7OH + 18OH^- \quad \text{(S7)}$$

$$CO_2 + H_2O + 2e^- \rightarrow HCOO^- + OH^- \quad \text{(S8)}$$

Carbon balance at the cathode

The faradaic efficiency of gaseous products was calculated using GC injections and measured outlet gas flowrate. The liquid products were quantified using H-NMR analysis. An overall carbon balance was performed, and the following equations were then used to calculate the volumetric flowrate of CO_2 reacting with hydroxide ions at the cathode.

$$x_{CO2,out} = 1 - (x_{CO} + x_{H2O} + x_{H2} + x_{C2H4} + x_{CH4}) \quad \text{(S9)}$$

After calculating the mole fractions of all gaseous products, the volumetric flow rate at the outlet of the reactor measured with the MFM and was used to calculate the moles of each product.

$$n_{CO} = \dot{V}_{outlet} \times x_{CO} \quad \text{(S10)}$$

$$n_{C2H4} = \dot{V}_{outlet} \times x_{C2H4} \quad \text{(S11)}$$

$$n_{CH4} = \dot{V}_{outlet} \times x_{CH4} \quad \text{(S12)}$$

$$n_{H2} = \dot{V}_{outlet} \times x_{H2} \quad \text{(S13)}$$

$$FE_{gas\ product} = \frac{n_{gas\ product} \times n^e \times F}{I} \times 100\ \% \quad \text{(S14)}$$

Here: $n_{gas\ product}$ - moles of produced gas product, n^e- number of electrons involved in CO_2RR, *F*- 96485 C/mol and *I* - applied current (in Amperes).

The following equations were then used to calculate the CO_2 consumption with OH^- ions by performing an overall carbon balance at the cathode.

$$\dot{V}_{CO_2\ to\ CO} = x_{CO} \times \dot{V}_{outlet} \quad \text{(S15)}$$

$$\dot{V}_{CO_2\ to\ C2H4} = x_{C2H4} \times \dot{V}_{outlet} \quad \text{(S16)}$$

$$\dot{V}_{CO_2\ to\ CH4} = x_{CH4} \times \dot{V}_{outlet} \quad \text{(S17)}$$

$$\dot{V}_{H_2} = x_{H_2} \times \dot{V}_{outlet} \quad \text{(S18)}$$

$$\dot{V}_{residual\ CO_2} = \dot{V}_{outlet} - \left(\dot{V}_{CO_2\ to\ CO} + \dot{V}_{CO_2\ to\ C2H4} + \dot{V}_{CO_2\ to\ CH4} + \dot{V}_{H_2}\right) \quad \text{(S19)}$$

$$\dot{V}_{CO_2\ to\ liquid\ prod} = \left((1 - x_{CO} - x_{H2}) \times \frac{j \times A}{n^e \times F}\ mol/s \times 22.4 \times 60 \times 1000\right)\ ml/min \quad \text{(S20)}$$

$$\dot{V}_{CO_2\ to\ gas} = \dot{V}_{CO_2\ to\ CO} + 2\left(\dot{V}_{CO_2\ to\ C2H4}\right) + \dot{V}_{CO_2\ to\ CH4} \quad \text{(S21)}$$

$$\dot{V}_{CO2\ to\ OH^-} = \dot{V}_{inlet} - \left(\dot{V}_{residual\ CO_2} + \dot{V}_{CO_2\ to\ gas\ products} + \dot{V}_{CO_2\ to\ liquids}\right) \quad \text{(S22)}$$

$$n_{CO2\ to\ OH^-} = \frac{\dot{V}_{CO2\ to\ OH^-}}{(24.42 \times 60 \times 1000)}\ mol/s \quad \text{(S23)}$$

$$\lambda_{stoich} = \frac{\dot{V}_{CO2,in}}{\dot{V}_{CO2,consumed}} \quad \text{(S24)}$$

$$Single\ pass\ CO_2\ conversion = \frac{\dot{V}_{CO2\ to\ C2+\ products}}{\dot{V}_{inlet}} \quad \text{(S25)}$$

$$CO_2\ utilization\ efficiency = \frac{\dot{V}_{CO2\ to\ gas} + \dot{V}_{CO2\ to\ liquid\ prod}}{\dot{V}_{CO2\ to\ gas} + \dot{V}_{CO2\ to\ liquid\ prod} + \dot{V}_{CO2\ to\ OH^-}} \quad \text{(S26)}$$

Moles of OH^- ions generated during the reaction can be calculated using Faraday's law. For every mole of OH^- ions produced during reactions (S7-S10), $1e^-$ is used. So,

$$n_{OH^-} = \frac{j_{geo} \times A}{1 \times F} = \frac{200\ mA cm^{-2} \times 5 cm^2}{96485} = 1.049 \times 10^{-5}\ moles \quad \text{(S27)}$$

CO utilization towards C_{2+} products

From equations S4-S6, the normalized partial current densities of hydrocarbons and oxygenates by the number of e^- transferred per CO reduced to a specific product is as follows:

$$CO_{generation\ rate}\ from\ CO_2RR = j_{CO} + \frac{j_{CH_4}}{4} + \frac{j_{C_2H_4}}{3} + \frac{j_{C_2H_5OH}}{3} + \frac{j_{CH_3COO^-}}{2} + \frac{j_{C_3H_7OH}}{3} \quad \text{(S28)}$$

$$CO_{dimerization\ rate} = \frac{j_{C_2H_4}}{3} + \frac{j_{C_2H_5OH}}{3} + \frac{j_{CH_3COO^-}}{2} + \frac{j_{C_3H_7OH}}{3} \quad \text{(S29)}$$

$$CO_{utilization\ rate} = \frac{CO_{dimerization\ rate}}{CO_{generation\ rate}} \quad \text{(S30)}$$

Supplementary Table 1 : Faradaic efficiency of all products obtained from ECO_2R for the three FFP at 200 mA/cm^2.

Flow field pattern and inlet flowrate	**FE CO (%)**	**FE C_2H_4 (%)**	**FE C_2H_5OH (%)**	**FE acetate (%)**	**FE n-propanol (%)**	**FE CH_4 (%)**	**FE $HCOO^-$ (%)**	**FE H_2 (%)**	**Total FE (%)**
Serpentine (10 sccm)	3.2	40.3	30.8	10.5	2.7	1.4	2.7	7.2	98.8
Serpentine (20sccm)	8.6	40.1	24.8	7.3	3.9	2.1	2.4	7.3	96.5
Serpentine (50 sccm)	12.2	39.1	20.3	4.4	4.6	0.3	6.9	6.8	94.9
Parallel (10 sccm)	3.1	32.0	22.4	15.9	1.7	9.0	3.8	10.7	98.6
Parallel (50 sccm)	5.1	36.2	22.1	14.7	2.3	3.1	2.7	10.8	97.0
Interdig. (10 sccm)	4.8	40.8	30.1	7.1	2.9	1.7	2.4	8.6	98.4

Supplementary Table 2: Calculated single pass CO_2 conversion and CO utilization to C_{2+} products at 200 mA/cm^2.

Inlet CO_2 flowrate (sccm)	**Single pass CO_2 conversion to C2+ (%)**	**Stoichiometric excess of CO_2 λ_{stoich}**	**CO generation rate (mA/cm^2)**	**CO dimerization rate (mA/cm^2)**	**CO utilization towards C_{2+} products (%)**
10	23.91	1.13	66.4	59.7	89.9
20	14.25	1.92	71.0	53.1	74.7
30	9.28	2.56	70.3	51.5	74.2
40	6.63	3.44	70.0	48.4	69.2
50	5.42	4.01	71.7	46.8	65.3
10 (parallel FFP)	19.38	1.16	63.9	53.4	81.5
50 (parallel FFP)	3.92	5.61	67.8	55.3	83.6

NMR analysis for liquid products

The NMR experiments were conducted with a Bruker-400 NMR spectrometer. A water suppression technique was applied to make the products' peaks more visible. 25 mM of maleic acid dissolved in D_2O was used as the internal standard. 550 µL of aliquot from the anolyte of the MEA cell was taken and added to 50 µL of maleic acid (25 mM) for NMR analysis.

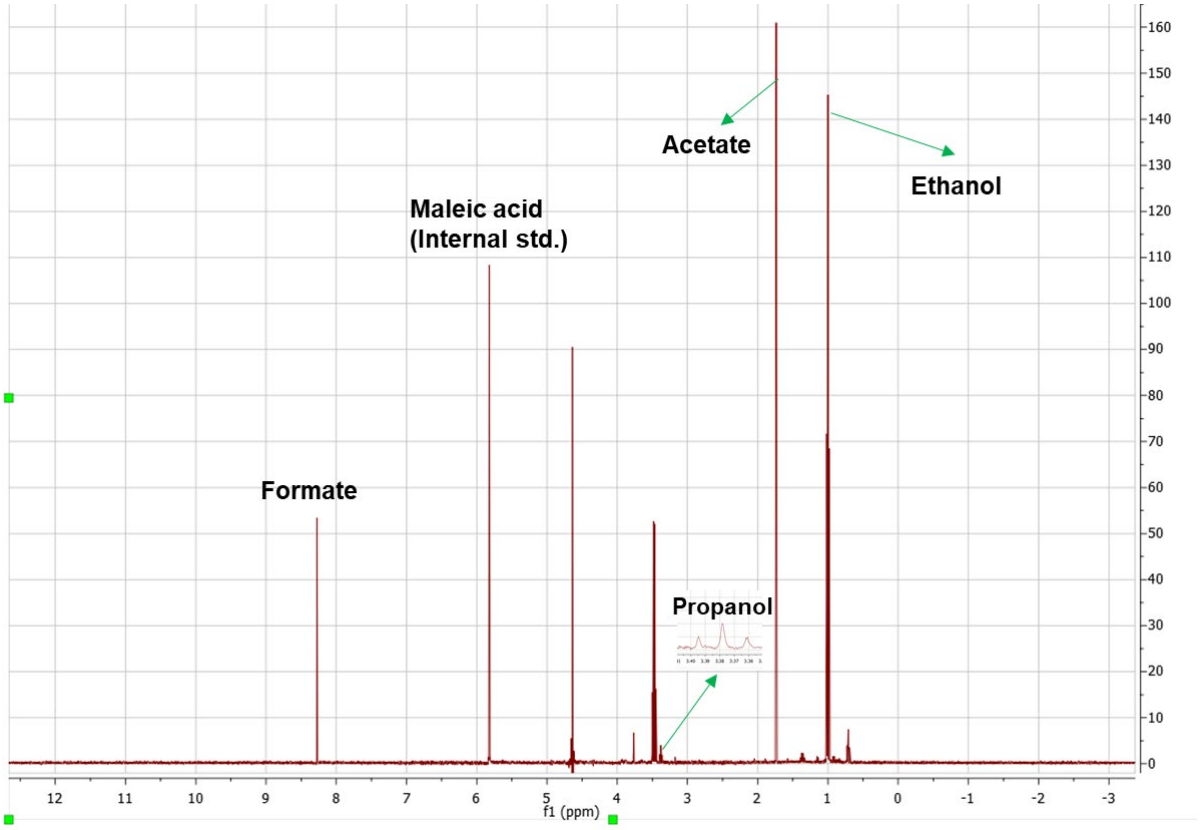

Supplementary Figure 11. H-NMR spectra of liquid products obtained from CO_2RR at an inlet flowrate of 10 sccm.

A total of 128 scans were performed for all tests and the molar concentration of liquid products were calculated using the equation:

$$C_x = \frac{I_x}{I_{std}} \times \frac{N_{std}}{N_x} \times C_{std} \quad \text{(S31)}$$

where, "C_x " is the molar concentration of the product, "I_x" is integral of the product, "I_{std}" is integral of the internal standard (maleic acid), "N_{std}" is the number of protons in maleic acid, "N_x" is the number of protons in the product, and "C_{std}" is the total concentration of maleic acid. "n" is the number of electrons for the specific product produced from CO_2. A sample NMR spectra for products obtained at the inlet flowrate of 10 sccm for the serpentine FFP is shown in Figure S10.

We also collected tiny liquid droplets from the cathode GDE into the liquid trap to quantify if any liquid products were present at the cathode side. The liquid drops from the liquid trap were diluted by adding MQ water to make a 10 mL solution and analyzed thereafter by NMR spectroscopy. NMR analysis showed only traces of ethanol with FE of 1-3 %, suggesting that most of the produced liquid products migrated to the anode through the AEM.

Supplementary Table 3. Liquid product selectivity produced from anode and cathode sides at different inlet CO_2 flowrates for the serpentine FFP.

Inlet flow rate of CO_2 (sccm)	FE of ethanol detected from anolyte (%)	FE of ethanol detected from cathode side (%)	Total FE of ethanol (%)
10	29.8	0.4	30.2
20	23.0	1.8	24.8
30	21.5	1.1	22.6
40	18.9	3.4	22.3
50	18.0	2.1	20.1

Proposed reaction pathways for CO_2 electroreduction to ethanol/ethylene

The following set of reactions are proposed for ethanol/ethylene pathway based on previous works by Goddard and co-workers[4].

1. $CO_2 + e^- \rightarrow *CO_2^-$ (S32)
2. $*CO_2^- + H_2O \rightarrow COOH^* + OH^-$ (S33)
3. $COOH^* + e^- \rightarrow *CO + OH^-$ (S34)
4. $*CO + *CO + H^+ + e^- \rightarrow *COCOH$ (S35)
5. $*COCOH + H^+ + e^- \rightarrow *COHCOH$ (S36)
6. $*COHCOH + 2(H^+ + e^-) \rightarrow CH_2CO$ (S37)
7. $CH_2CO + H^* \rightarrow CHCHOH^*$ (hydrogenation to ethanol) (S38)
8. $CH_2CO + e^- \rightarrow CCH^* + OH^-$ (dehydroxylation to ethylene) (S39)
9. $CH_2CO + OH^- \rightarrow CH_3COO^-$ $(solution\ reaction)$ (S40)

The reaction of intermediate $HOCCH^*$ through a hydrogenation pathway (Eq.S38) or dehydroxylation pathway (Eq.S39) determines ethanol vs ethylene pathway. This means that the concentration of $^*H$ at the catalyst surface is an important metric in addition to $^*CO$ for ethanol formation.

SEM analysis of Cu coated GDL before and after CO_2RR

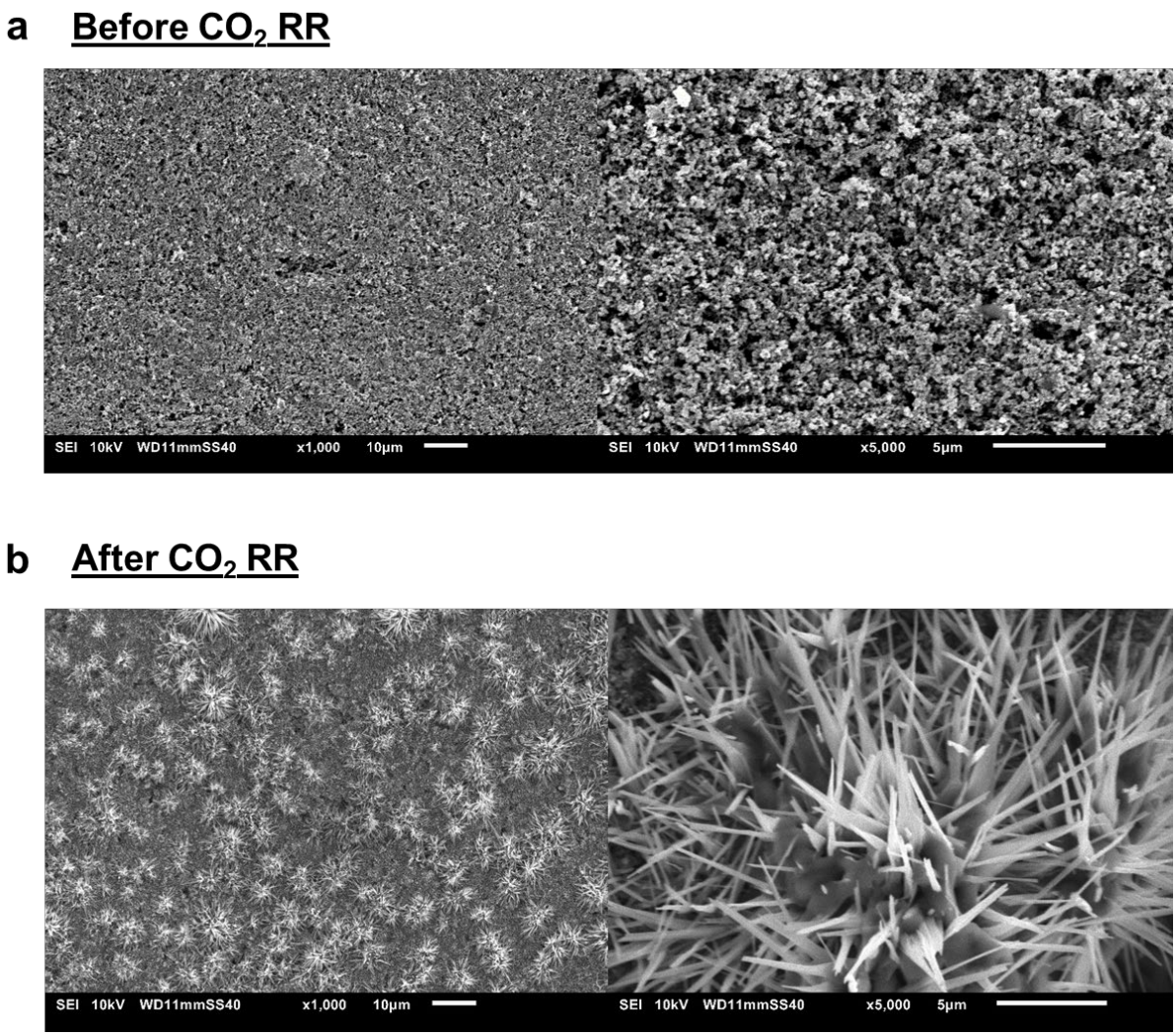

Supplementary Figure 12. SEM images of Cu catalyst layer sputtered on Sigracet 38 BC gas diffusion layer (a) before and (b) after 1 h of CO_2 electrolysis.

Model description

A 3D geometry of the cathode compartment (5cm^2 area) comprising of the three flow channel designs were modelled with the same length (2.1 cm), width (1 mm) and depth (1 mm) in COMSOL Multiphysics 5.5, similar to our previous work. A carbon GDL of dimensions (2.25 cm x 2.25 cm x 0.325 cm) was modelled and placed in contact with the flow field pattern with each one consisting of 11 channels and 10 ribs. The numerical simulations were performed using a MUMPS general solver with a relative tolerance of 0.001 to calculate the CO_2 concentration gradient in the gas channel and catalyst surface.

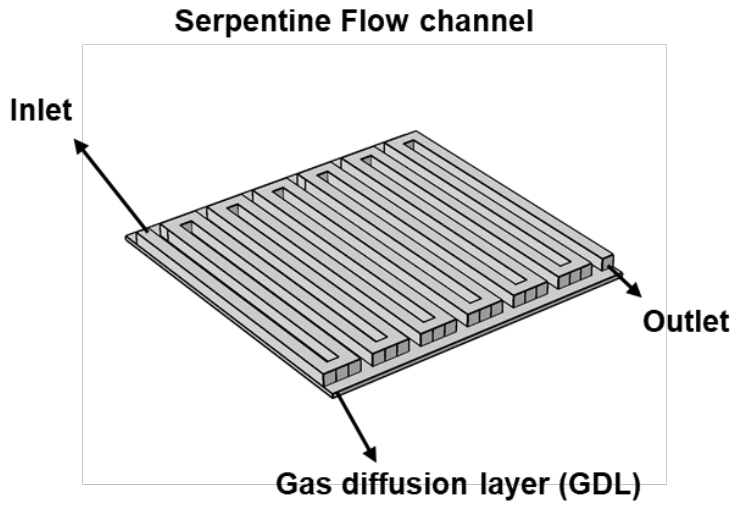

Supplementary Figure 13. 3D transport model of the cathode compartment of MEA cell modelled in COMSOL Multiphysics. Shown here is the serpentine flow field pattern.

All parameters used in the model were taken from the experimental conditions and the properties of the Sigracet 38BC GDL. The following assumptions were made in the model:

i) The system operates at steady-state conditions.

ii) Carbon GDL is assumed to be isotropic with constant porosity and permeability since the in-plane diffusion is higher than the through plane diffusion.

iii) Both diffusion and convection from the channel to the catalyst surface are considered

iv) A uniform current distribution is assumed at the catalyst surface.

v) Isothermal at 298 K with no thermal diffusion gradients

Brinkmann equation and mixture diffusion model

The fluid flow in the flow channels were modelled Navier stokes equation and flow through the GDL using Brinkmann equation. A no-slip boundary condition was imposed on the channel walls. A slip condition was used at the channel-GDL interface since the normal component of velocity is zero at this interface. Single phase compressible flow was assumed. An inlet boundary condition was given by a normal inflow velocity defined by the flowrate ($\dot{V}_{in}$) over inlet cross sectional area of the channel (Dirichlet boundary condition). $\dot{V}_{in}$ was fixed at 10 sccm as used in the experiments. Constant pressure at the outlet of the cell (1 atm) was used as the boundary condition at the outlet (Neumann boundary condition) with the suppression of backflow.

The Brinkman equation solves for the velocity and pressure distribution in the GDL. It was coupled with the mixture diffusion model which takes into account of diffusion and convection through the GDL. All parameters used in the model can be found in Table 5. For the meshing, a free tetrahedral mesh with a fine mesh size was used for the channels and a swept mesh was used for the GDL (98023 domain elements, 24196 domain elements and 2894 edge elements). The velocity and pressure field in the gas channels were solved using:

$$\rho(\mathbf{u}\cdot\boldsymbol{\nabla})\mathbf{u} = \boldsymbol{\nabla}\cdot\left[-p\boldsymbol{I} + \mu(\nabla\mathbf{u} + (\nabla\mathbf{u})^{\mathrm{T}}) - \tfrac{2}{3}\,\mu(\nabla\cdot\mathbf{u})\mathbf{I}\right] + \mathrm{F} \tag{S41}$$

$$\nabla\cdot(\rho\mathbf{u}) = 0 \tag{S42}$$

In the GDL, the velocity and pressure was calculated using:

$$\tfrac{1}{\epsilon_p}\rho(\mathbf{u}\cdot\nabla)\mathbf{u}\tfrac{1}{\epsilon_p} = \nabla\cdot\left[-p\mathbf{I} + \mu\tfrac{1}{\epsilon_p}(\nabla\mathbf{u} + (\nabla\mathbf{u}^{\mathrm{T}}) - \tfrac{2}{3}\mu\tfrac{1}{\epsilon_p}(\nabla\cdot\mathbf{u})\mathbf{I}\right] - \left(\mu\kappa^{-1} + \tfrac{Q_m}{\epsilon_p^2}\right)\mathbf{u} + \mathrm{F} \tag{S43}$$

$$\nabla\cdot(\rho\mathbf{u}) = Q_m \tag{S44}$$

In these equations,

ρ is the density of the fluid, μ is the dynamic viscosity of the fluid, p is the pressure, $\mathbf{u}$ is the velocity, F is the force term, κ is the permeability of the GDE, ϵ_p is the porosity of the GDE and Q_m is the mass source.

Mixture diffusion model

To solve for the species transport in the system, a mixture diffusion model was used. We accounted for only 2 gas species which are CO_2 at the inlet and C_2H_4 as the outlet since it was the dominant gas product. The molar flux of the species were calculated using the following equations:

$$\nabla \cdot j_i + \rho(\mathbf{u} \cdot \nabla)\omega_i = R_i \tag{S45}$$

$$N_j = j_i + \rho \mathbf{u} \omega_{\boldsymbol{i}} \tag{S46}$$

$$\boldsymbol{j}_i = -(\rho D_i^m \nabla \omega_i + \rho \omega_i D_i^m \frac{\nabla M_n}{M_n}) \tag{S47}$$

$$R_i = \frac{v_i i_v}{nF} + j_{CO2\ to\ OH^-} \tag{S48}$$

Here:

N is the total flux vector of species i, R_i is the reaction rate for species i, **u** is the fluid velocity, $\mathbf{j}_i$ is the relative mass flux due to molecular diffusion of species i, ω_i is the mass fraction of species i, i_v is the volumetric current density, F- Faraday's constant. D_i is the binary diffusivity of CO_2 with respect to C_2H_4 and was calculated using Fuller correlation.

<u>CO_2 consumption calculation</u>

Electrochemical reduction of CO_2 to C_2H_4 was modelled which is a $12e^-$ reduction reaction:

$$CO2\ RR\ to\ C_2H_4 :\ 2CO_2 + 8H_2O + 12e^- \rightarrow C_2H_4 + 12OH^- \tag{S49}$$

The CO_2 consumption to CO_2RR was calculated based on number of electrons involved for each molecule of CO_2 for the different products and their corresponding FEs. The FE of various products obtained from experiments was used for calculating CO_2 consumption.

$$z_{avg} = \left\{ \sum \left(\frac{FE_{C_i}}{FE_{CO2RR}} \times \frac{z_{e,C_i}}{\nu_{CO_2}} \right) \right\} \tag{S50}$$

where z_{avg} is the average number of electrons utilized for CO_2RR, z_{e,C_i} is the number of electrons involved in CO_2RR to the specific product C_i (equations S2-S8), ν_{CO2} is the stoichiometric coefficient of CO_2 for the specific CO_2RR.

The moles of CO_2 lost to OH^- ions calculated experimentally using carbon balance (Eq. S22) was used in the model and assumed to occur homogenously throughout the catalyst layer. Using z_{avg} calculated from Eq. S50, an equivalent current density was calculated and incorporated into the model for calculating CO_2 consumption.

$$j_{CO2\ to\ OH^-} = \frac{n_{CO2\ to\ OH^-} \times z_{avg} \times F}{A} \quad \text{(S51)}$$

$$j_{total} = j_{CO2RR} + j_{CO2\ to\ OH^-} \quad \text{(S52)}$$

Here, $j_{CO2\ to\ OH^-}$ is the equivalent current density per mole of CO_2 consumed due to reaction with OH^- ions, F is Faraday's constant and A is the geometric area of the GDE (5.06 cm^2).

Calculated CO_2 concentration at the G-L interface for ECO_2R at 10 sccm and 200 mA/cm^2

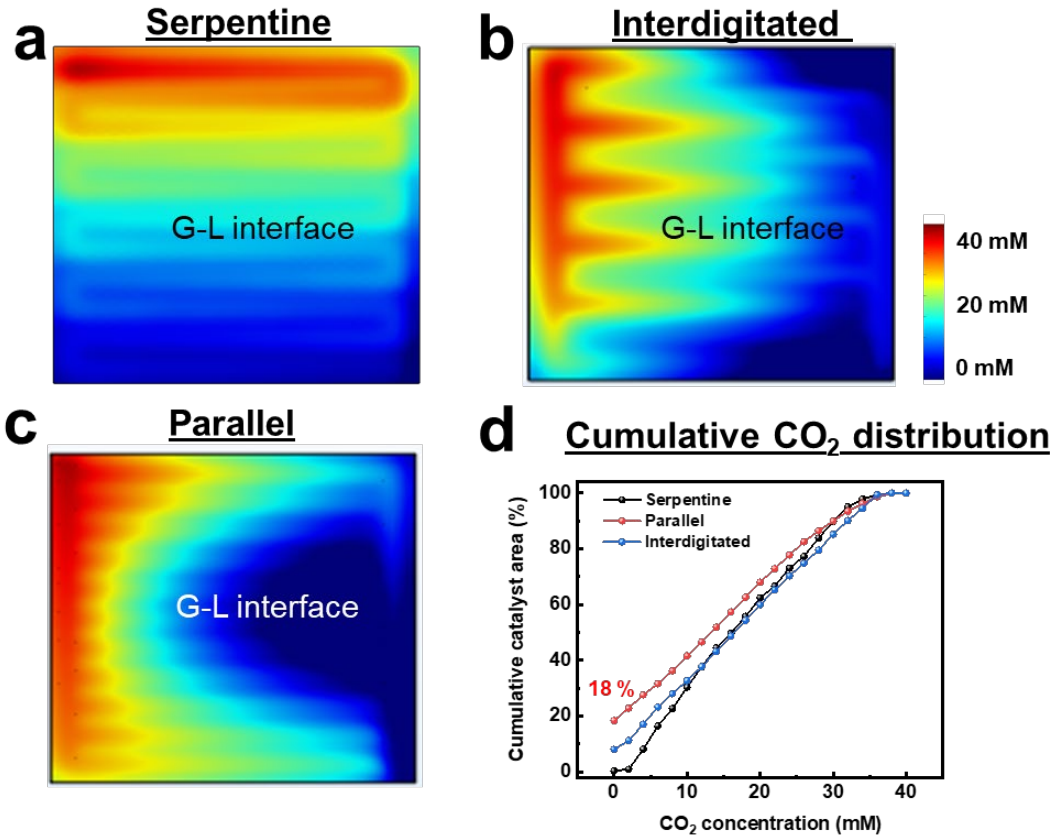

Supplementary Figure 14. Calculated gas phase CO_2 concentration at the G-L interface for (a) Serpentine, (b) Parallel and (c) Interdigitated flow field patterns at an inlet flowrate of 10 sccm and 200 mA/cm^2. (d) Cumulative CO_2 distribution at the G-L interface for all three FFPs.

Supplementary Figure 14(a-c) shows the calculated CO_2 concentration gradients (gas phase) at the gas-liquid interface. At the catalyst-membrane/electrolyte interface, Henry's law can be used to calculate CO_2 concentration in the liquid phase as shown in a number of previous reports. Using this, the actual CO_2 concentration at the catalyst-electrolyte interface will be slightly lower than that predicted in Supplementary Figure 14, but the trends associated with the three flow fields will remain similar in terms of CO_2 access throughout the 5 cm^2 electrode will be similar.

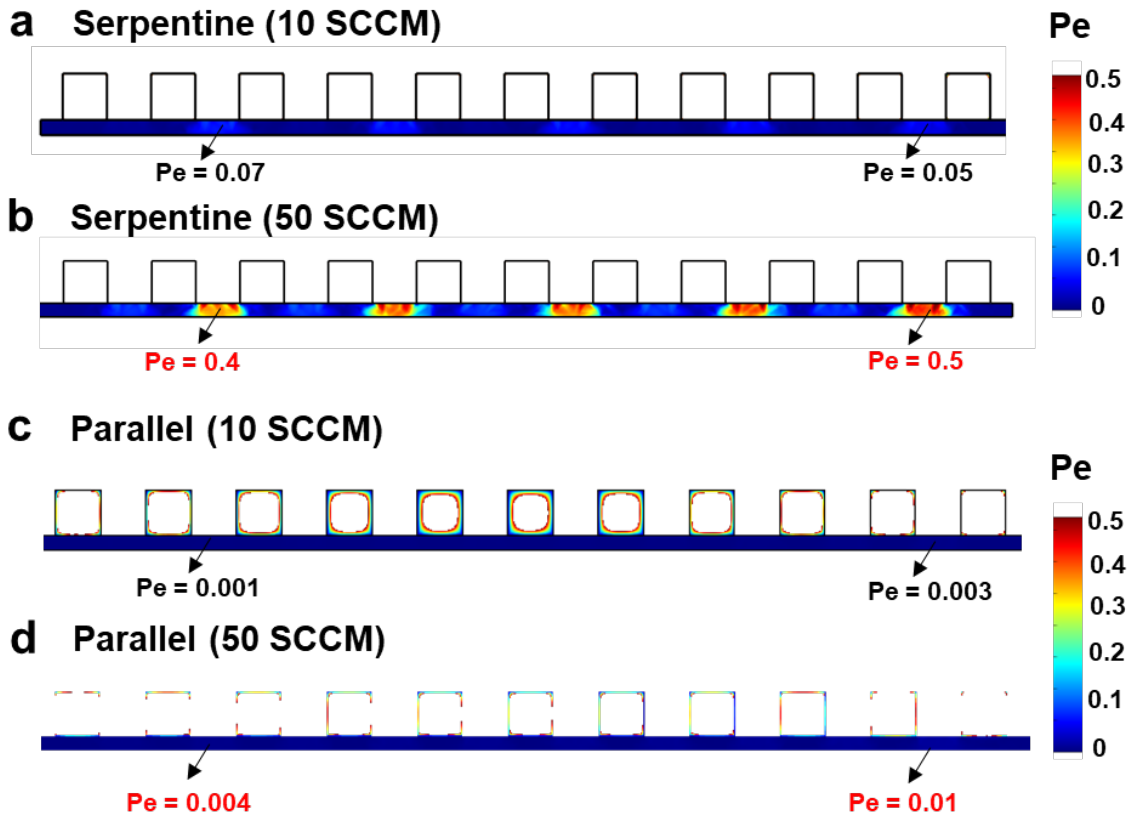

Supplementary Figure 15: Peclet numbers inside the GDE at inlet flowrates of 10 and 50 SCCM using (e) Serpentine and (f) Parallel FFP.

The Pe number in Supplementary Figure 14 (e) and (f) were calculated from the modelling results using the following equation:

$$Pe = \frac{advective\ transport\ rate}{diffusive\ transport\ rate} = \frac{2 \times u_{GDL} \mathrm{L}}{D_{CO_2 to\ C_2H_4}}$$

Here: Pe is the calculated peclet number, u_{GDL} is the velocity through the GDE, L is the characteristic length which is = 2 x thickness of GDE and $D_{CO_2 to\ C_2H_4}$ is the binary diffusivity of CO_2 w.r.t to C_2H_4.

Supplementary Figure 15 shows the 2D Pe inside the GDE between every gas flow channel where under-rib advection/convection is found to be present. We calculate a Pe of 0.4-0.5 for serpentine FFP at 50 SCCM which is an order of magnitude higher than 10 SCCM (Pe = 0.05-0.07). A higher Pe at

50 SCCM shows the lower CO residence time observed in the electrochemical and RTD tests as compared to 10 SCCM case.

Similarly, Pe numbers are an order of magnitude lower for the parallel FFP when compared to the serpentine case. This shows the benefit of parallel flow field in eliminating any advective transport completely, resulting in higher residence time of CO inside the catalyst layer as evident from electrochemical and RTD tests.

Calculated CO_2 concentration at the G-L interface for CO_2ER at 50 sccm and 200 mA/cm^2

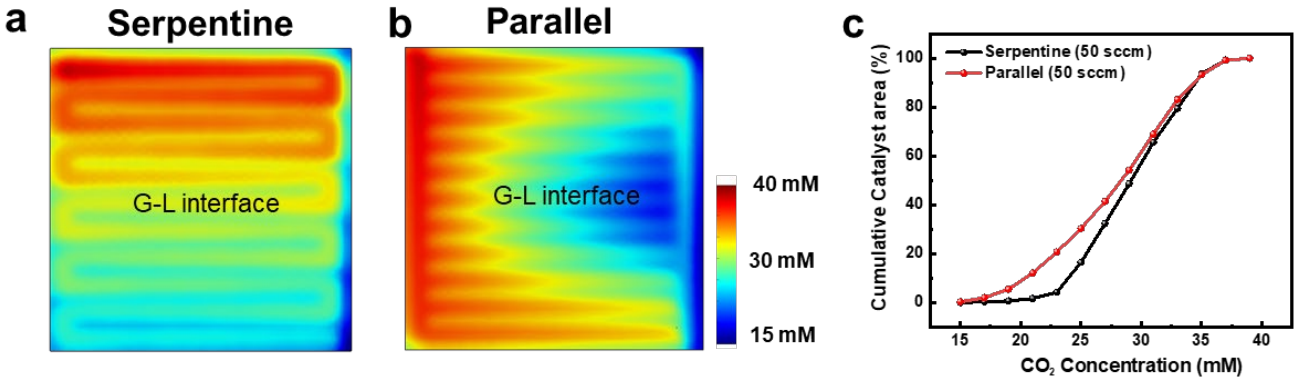

Supplementary Figure 16. Calculated gas phase CO_2 concentration at the G-L interface for (a) Serpentine, (b) Parallel flow field design at an inlet flowrate of 50 sccm and 200 mA/cm^2. (c) Cumulative CO_2 distribution for the two FFPs.

Supplementary Table 4: Calculated pressure drop and gas phase CO_2 concentration at the G-L interface from the model for the three flow field patterns.

Flow field pattern	**Inlet CO_2 flowrate (sccm)**	**ΔP b/w inlet and outlet (Pa)**	**Avg. velocity in gas channels (mm/s)**	**Avg. velocity through GDL (mm/s)**	**Avg. [CO_2] at G-L interface (mM)**
Serpentine	10	22.2	1.3	1.1	17.8
Parallel	10	1.3	0.5	0.03	15.2
Interdigitated	10	15.2	0.6	1.7	15.6
Serpentine	50	112.4	5.7	5.7	30.9
Parallel	50	6.4	1.9	0.125	28.9

Supplementary Table 5 : Parameters used in the 3D mass transport and fluid flow model

Parameter	Symbol	Value	Units	Reference
Temperature	T	298	K	This work
Reference pressure	P	1	atm	This work
Diffusivity of CO_2 into C_2H_4	$D_{CO2\text{-}C2H4}$	1.245×10^{-5}	$m^2 s^{-1}$	This work
Porosity of GDE	eps_gdl	0.8	$-$	[2]
Permeability of GDE	kappa_gdl	7×10^{-12}	m^2	[2]
Inlet flowrate	Q_{sccm}	10	sccm	This work
Applied current density	i_{loc}	-(2000 + $j_{CO2\ to\ OH-}$)	Am^{-2}	This work
Length of channel	l	2.1	cm	This work
Width of channel	w	1	mm	This work
Depth of channel	h_ch	1	mm	This work
Thickness of GDE	dep_gdl	325	µm	[2]
Dynamic viscosity of CO_2	mu	1.47×10^{-5}	Pa.s	[1]
Average number of electrons	n_{avg}	5.52	-	This work

CO electrolysis

Electrochemical CO reduction tests were performed at 200 mA/cm^2 and an inlet flow rate of 20 sccm, inside a fumehood containing potentiostat, mass flow meter and gas chromatography setup. All experiments for the three flow field patterns were repeated twice to verify reproducibility.

Supplementary Table 6 : Selectivity of products obtained from E COR for the three FFP at 200 mA/cm^2.

Flow field pattern	**FE C_2H_4 (%)**	**FE C_2H_5OH (%)**	**FE acetate (%)**	**FE n-propanol (%)**	**FE CH_4 (%)**	**FE H_2 (%)**
Serpentine	30.84	14.43	32.9	1.5	2.38	5.4
Parallel	29.3	15.5	31.7	1.7	4.15	9.5
Interdigitated	35.01	18	22.0	2.4	1.9	7.8

Supplementary Table 7: Comparison of performance metrics for ethylene production from ECO_2 RR and ECOR at a geometric current density of 200 mA/cm^2. Results of interdigitated FFP are used since ethylene selectivity obtained were the highest using this FFP for both electrochemical reactions.

Reaction	**Full cell voltage obtained (E_{cell})**	**TD Cell voltage for C_2H_4 (E^0_{cell,C_2H_4})**	**TD Cell voltage for C_2H_5OH OH (E^0_{cell,C_2H_5OH})**	**FE of C_2H_4 (%)**	**FE of ethanol (%)**	**Electrical Energy efficiency for ethylene + ethanol, (eEE) (%)**
CO_2 ER	2.81	1.15	1.14	41.5	29.5	28.96
CO ER	2.47	1.06	1.04	35.0	20	23.42

The electrical energy efficiency for ethylene+ethanol production is calculated using the following equation :

$$eEE = \left(\frac{FE_{C2H4} \times E^0_{cell,C_2H_4}}{E_{cell}}\right) + \left(\frac{FE_{C2H5OH} \times E^0_{cell,C_2H_5OH}}{E_{cell}}\right) \quad \text{(S53)}$$

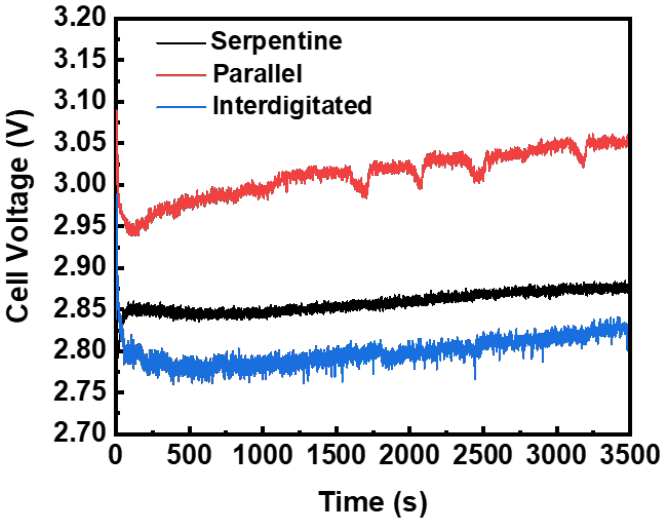

Supplementary Figure 17. Cell voltage for ECO_2R for the three FFP at an inlet flowrate of 10 sccm for 1 hr electrolysis.

Blank RTD measurements

For the pulse RTD tests, the contribution of tubing from the tracer inlet to mass spectrometer can contribute to measured residence time for RTD tests. To account for this, blank RTD tests were performed without any MEA cell, connecting all the tubing together. The measured time for these blank tests were taken to calculate actual mean residence time inside the reactor as shown in Figure 1c in the main MS.

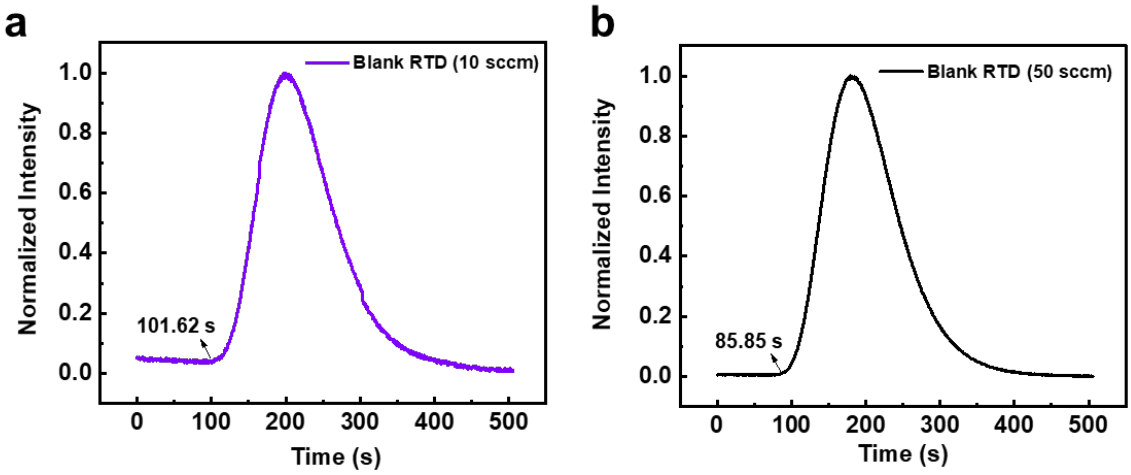

Supplementary Figure 18. Blank RTD tests performed at tracer flowrates of 10 and 50 SCCM. The contribution of tubing was 101.62 s and 85.85 s at 10 and 50 SCCM respectively.

Acetate formation rates during ECO_2R and ECO RR

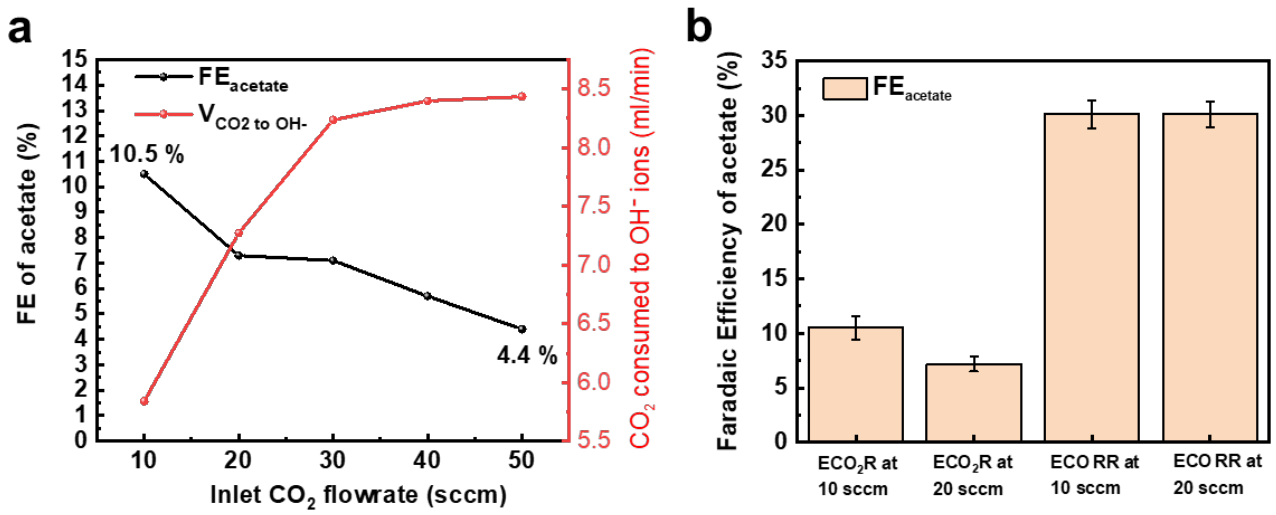

Supplementary Figure 19: (a) FE of acetate during ECO_2R at various inlet CO_2 flowrates and corresponding CO_2 lost to OH^- ions during reaction. **(b)** Comparison of FE of acetate during ECO_2R and ECO R at inlet flowrates of 10 and 20 sccm.

Energy requirements for CO_2 electrolysis and ethanol dehydration reaction

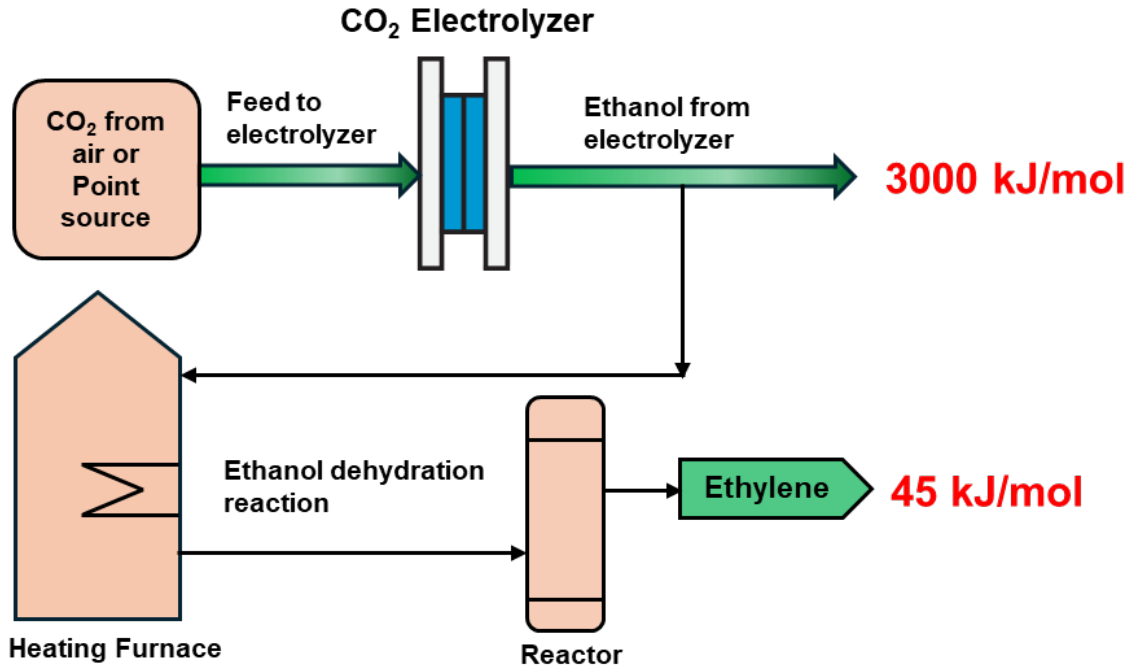

Supplementary Figure 20: Simplified schematic of the energy requirements involved in a CO_2 electrolyzer producing ethanol and subsequent ethylene generation from ethanol dehydration reaction.

EIS analysis to calculate ECSA of Cu GDE

In order to determine the electrochemical active surface area (ECSA) of Cu coated GDL, we measured performed electrochemical impedence spectroscopy (EIS) at a current density of -10 mA/cm^2 before CO_2 electrolysis. The frequency of EIS was varied from 10000 Hz to 0.1 Hz at an amplitude of 10 mV (RMS).

The obtained Nyquist plots were fitted using Randles circuit comprising of one resistor in parallel with a series of resistor and a constant phase element (CPE) and double layer capacitance was calculated using the following equation:

$$C_{dl} = \frac{(\gamma_0 \times R_{ct})^{\frac{1}{\alpha}}}{R_{ct}}$$

Here: C_{dl} is the double layer capacitance, R_{ct} is the charge transfer resistance, γ_0 is the capacitance and α is the exponential term which is 0 for pure resistor and 1 for pure capacitor.

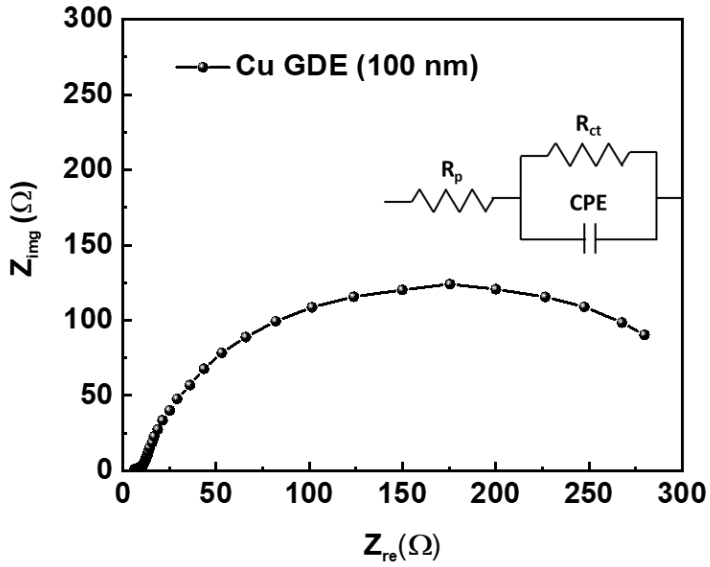

Supplementary Figure 21: Nyquist plot of EIS for a Cu GDE performed at a reduction current density of 10 mA/cm^2.

From the Nyquist plot obtained in Supplementary Figure 20, the obtained spectra was fitted with the Randles circuit as shown and fitted with ZSimpwin software. The obtained parameters were as follows:

$$R_p = 0.33\ \Omega\,, \gamma_0 = 0.01108, \alpha = 0.78\ and\ R_{ct} = 2.003\ \Omega$$

$$C_{dl} = \frac{(\gamma_0 \times R_{ct})^{\frac{1}{\alpha}}}{R_{ct}} = \frac{(0.01108 \times 2.003)^{\frac{1}{0.78}}}{2.003} = 0.0038567\ F = 3.85\ mF$$

For a 5 cm^2 geometric area of the Cu GDE, the specific capacitance is then:

$$C_{dl} = \frac{3.85\ mF}{5\ cm^2} = \mathbf{0.385\ mF/cm^2}$$

Based on previous reports, the specific capacitance of a Cu metal is 30 μF/cm^2. Using this, the roughness factor (RF) for the Cu GDE used here is :

$$RF = \frac{0.385\ mF}{30\mu F\ cm^{-2}} = \mathbf{25.6}$$

The electrochemical active surface area of Cu GDE used in CO_2 electrolysis can be estimated using this value and ECSA normalized current densities can be used to translate the residence time effects for other Cu based catalysts prepared by other catalyst preparation techniques.

Non-normalized RTD data

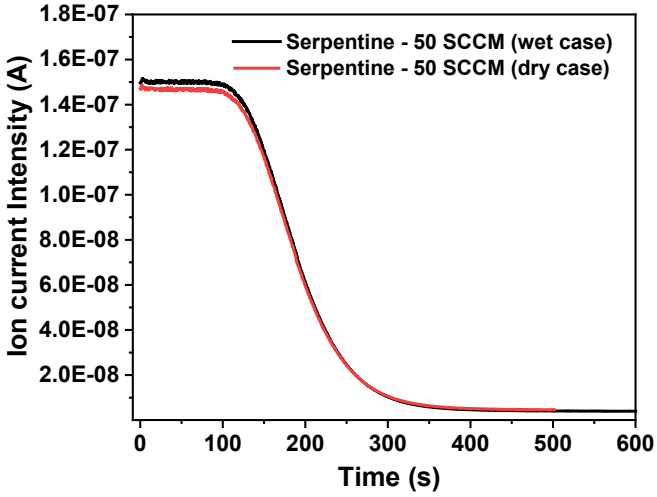

Supplementary Figure 22: Non-normalized CO RTD data for wet case (with Zirfon membrane) and dry case (without Zirfon membrane) using a serpentine flow field at a flowrate of 50 SCCM.

RTD of CO for all three flow field patterns

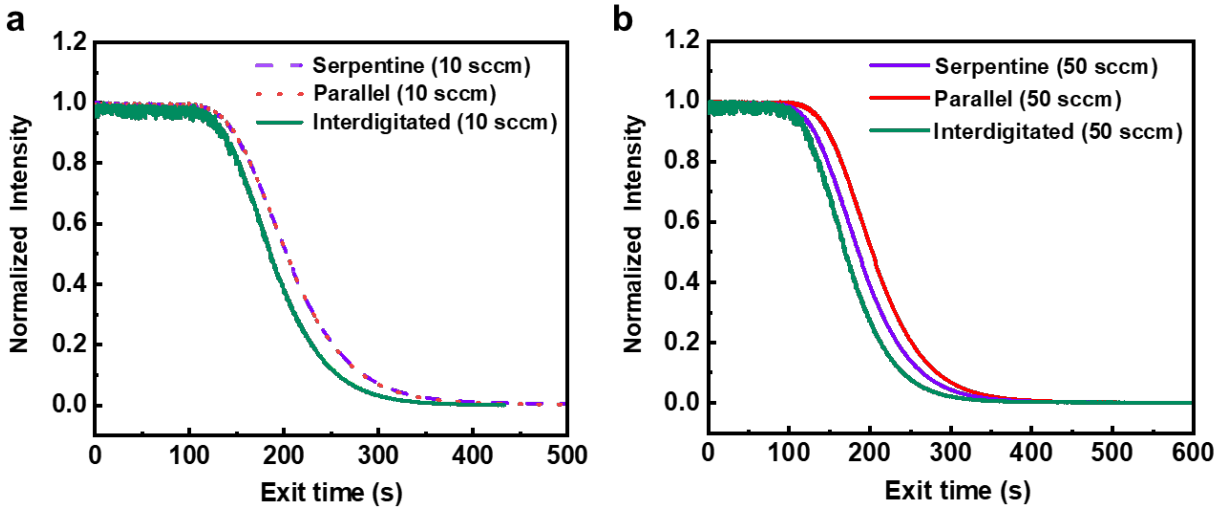

Supplementary Figure 23: Negative tracer results for the serpentine, parallel and interdigitated FFP at inlet flowrates of 10 and 50 SCCM with a wetted Zirfon membrane pressed against the carbon GDL.

References

[1] E. L. Cussler, *Diffusion, mass transfer in fluid systems*, Cambridge University Press, Cambridge Cambridgeshire ; New York, 1984.

[2] R. Schweiss, C. Meiser, T. Damjanovic, I. Galbiati and N. Haak, *SIGRACET® Gas Diffusion Layers for PEM Fuel Cells, Electrolyzers and Batteries (White Paper)*, SGL CARBON GmbH, 2016.

[3] Xiao, H., Cheng, T. & Goddard, W. A. Atomistic mechanisms underlying selectivities in C1 and C2 products from electrochemical reduction of CO on Cu(111). J. Am. Chem. Soc. 139, 130–136 (2017).